IMA Journal of Applied Mathematics (2016) **81**, 1–25
doi:10.1093/imamat/hxv023
Advance Access publication on 18 August 2015

A theoretical model of an ultrasonic transducer incorporating spherical resonators

Alan J. Walker*
School of Science and Sport, University of the West of Scotland, Paisley, PA1 2BE, UK
*Corresponding author: alan.walker@uws.ac.uk

and

Anthony J. Mulholland
Department of Mathematics and Statistics, University of Strathclyde, Glasgow, G1 1XH, UK

[Received on 6 September 2013; revised on 16 December 2014; accepted on 18 July 2015]

This article considers the theoretical modelling of a novel electrostatic transducer in which the backplate consists of many spherical resonators. Three analytical models are considered, each of which produce impedance profiles of the device, in addition to transmission voltage responses and reception force responses, all of which closely agree. Design parameters are then varied to investigate their influence on the resonant frequencies and other model outputs.

Keywords: transducer; spherical resonator; Helmholtz; ultrasound.

1. Introduction

Ultrasound is employed in a variety of technological applications which include penetration of a medium and analysis of the reflected wave (medical imaging and non-destructive evaluation) and focused energy supply (industrial cleaning and therapeutic ultrasound) (see Ladabaum *et al.*, 1998; Leighton, 2007). Electrostatic ultrasonic transducers are used for the detection and generation of ultrasonic waves (see Manthey *et al.*, 1992). These transducers consist of a thin dielectric membrane stretched across a conducting backplate. This backplate is often rough or grooved in order to trap air beneath the membrane and reduce the membrane's rigidity (see Schindel *et al.*, 1995). Recently, backplates have been designed with machined cavities with acoustic amplifying conduits emanating from the cavity (see Campbell *et al.*, 2006; Walker *et al.*, 2008; Walker & Mulholland, 2010). Issues such as manufacturing tolerances can arise in these designs due to the dependence of the cavity and conduits' dimensions on the transducer's resonating frequencies. This is one factor which can affect the performance of a transducer; other factors include the membrane's thickness and size (see Rafiq & Wykes, 1991; Noble *et al.*, 2001), the voltages applied (see Bayram *et al.*, 2003) and issues which arise concerning the impedance matching into air or any other fluid (see Alvarez-Arenas, 2004; Saffar & Abdullah, 2012). Conventionally, the propagation of ultrasound from a transducer into a material which is under inspection has been facilitated by the use of a liquid or gel couplant (see Lynnworth, 1965; Reilly & Hayward, 1991; Manthey *et al.*, 1992).

Airborne ultrasound has many applications in non-destructive testing and capacitive ultrasonic transducers perform well in such applications due to good impedance matching of the dielectric membrane to the air load. Recently, methodologies for manufacturing backplates have been developed that are based

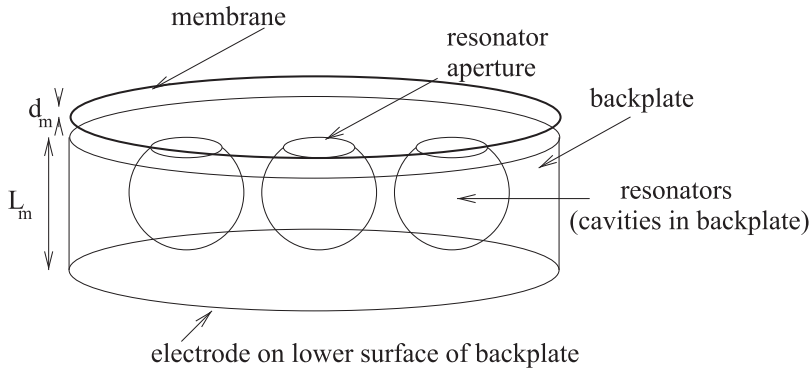

FIG. 1. A schematic representation of the electrostatic transducer where the spacing between the membrane and the backplate and the size of the resonators have been exaggerated. In practice, there would be tens or hundreds of these resonators in a square or circular-like lattice. The membrane displacement is zero unless it lies above one of the resonator apertures.

on depositing ternary solutions, one solvent and two solute polymers, onto an electrically conducting substrate (or a non-conductive substrate which is subsequently electroded). During the deposition process, the polymers undergo phase separation and the cavities can then be created by selective dissolution of one polymer phase. The dimensions of the cavities and their spatial distribution can be controlled by selection of the solutes and solvent and the rate of solvent evolution during the deposition process. This process can be used to make Helmholtz resonator-like cavities in the backplate which can be used to tune the resonator to a specific frequency (Mackie & O'Leary, 2012).

This article considers the theoretical modelling of such an ultrasonic transducer. The design consists of a metalized Mylar membrane stretched over a conducting backplate which incorporates evenly spaced spherical cavities formed by the process described above. Figure 1 provides a schematic of the cavity design. The important outputs from the model are the mechanical impedance and the transmission and reception sensitivities of the device. Three models are proposed and compared; a 1D (in space) model where the membrane is considered to operate as a damped harmonic oscillator, a membrane model where the dominant restoring force comes from the tension applied, and a plate model where the restoring forces comes from internal stiffness. The form of the 1D model is similar in form to the model proposed by Walker & Mulholland (2010) where fluidic amplification was implemented. The membrane and plate models are based on the work by Caronti *et al.* (2002) which considers the modelling of a capacitive micromachined ultrasonic transducer which incorporates a machined cavity in the backplate. The main difference from these articles is the form of the drag forces on the membrane which is calculated from Helmholtz resonator theory.

In Section 2 each mathematical model is described. The differential equations are solved via two different techniques which provide the mechanical impedance profile of the device. Derivation of the transmission voltage response (TVR) and reception force response (RFR) is also provided. Section 3 presents a comparison between the three different models. It is shown that the proposed models are in agreement with each other and they predict an operating frequency of around 1.5 MHz. Then, in Section 4, design parameters related to the spherical resonators are varied in order to ascertain their influence on the resulting resonating frequency of the device. It is found that selecting specific design parameter values can drastically alter the device operating performance. Conclusions and discussions are then provided in Section 5.

2. Analytical models of an electrostatic ultrasonic transducer incorporating Helmholtz resonators

To begin, the radiation impedance for one spherical resonator is computed and then used to provide a lumped impedance profile for the full backplate. This is then inserted into the three derived models which are then solved for the mechanical impedance profile of the device. The transmission and reception sensitivities are then derived.

2.1 *Backplate impedance model*

A single Helmholtz resonator with a radius r_r and an aperture of radius r_a, as shown in Fig. 2, is considered. For the frequencies of interest, it is assumed that $\lambda \gg \sqrt[3]{V_r}$ and $\lambda \gg \sqrt{S_a}$, where λ is the wavelength of the sound in the resonator, V_r is the volume of the resonator and $S_a = \pi r_a^2$ is the area of the aperture. This aperture radiates sound, providing a radiation resistance and a radiation mass. The compression of the fluid in the resonator provides a stiffness s_r. If it is assumed that the aperture radiates sound in the same manner as an open-ended pipe, the radiation resistance R_r is given by Kinsler *et al.* (2000, p. 285)

$$R_r = \frac{\rho_a c r_a^2 \pi^3}{\lambda^2}, \tag{2.1}$$

where ρ_a is the density of the fluid in the resonator and c is the speed of sound in the resonator. The thermoviscous resistance, R_ω, can also be included in the formulation of the impedance, where (Kinsler *et al.*, 2000, p. 285)

$$R_\omega = 2m' c \alpha_\omega, \tag{2.2}$$

and α_w is the absorption coefficient for wall losses, given by

$$\alpha_w = \frac{1}{r_a c}\left(\frac{\eta\omega}{2\rho_a}\right)^{1/2}\left(1 + \frac{\gamma_\omega - 1}{\sqrt{Pr}}\right), \tag{2.3}$$

with η being the coefficient of shear viscosity, ω the angular frequency, $\gamma_\omega \approx 8/\pi$ an attenuation coefficient (see Kinsler *et al.*, 2000, p. 213), and Pr being the Prandtl number. The total effective mass m' of the aperture is given by

$$m' = \rho_a S_a L', \tag{2.4}$$

where

$$L' \approx L + 1.6 r_a, \tag{2.5}$$

is the effective length of the neck of the resonator, with L being the actual length of the neck of the resonator. For the main, L is set equal to zero, other than in Section 4.3.

To determine the stiffness of the resonator(s), an airtight membrane over the aperture of the resonator is considered. When the membrane is pushed in a distance ψ, the volume of the resonator is changed by $\Delta V_r = -S_a\psi$, resulting in a pressure increase of $p_r = \rho_a c^2 S_a \psi / V_r$. The force required to maintain this displacement is given by $f_r = S_a p_r = s_r \psi$ and therefore the effective stiffness is

$$s_r = \frac{\rho_a c^2 S_a^2}{V_r}. \tag{2.6}$$

The instantaneous complex driving force produced by a pressure wave of amplitude P_i impinging on the resonator aperture is $f(t) = S_a P_i \, \mathrm{e}^{\mathrm{i}\omega t}$, where $\mathrm{i} = \sqrt{-1}$ and t is time. The resulting equation for the

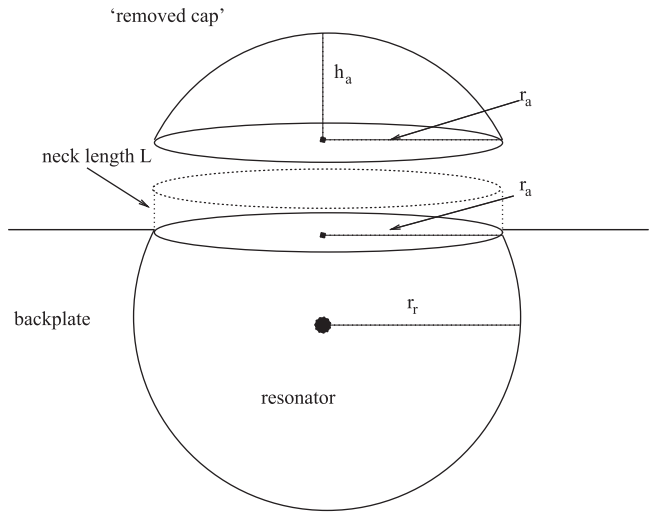

FIG. 2. A schematic representation of a single resonator, manufactured by depositing ternary solutions, one solvent and two solute polymers, onto an electrically conducting substrate. During the deposition process the polymers undergo phase separation and the cavities can then be created by selective dissolution of one polymer phase. The dimensions of the cavities and their spatial distribution can be controlled by selection of the solutes and solvent and the rate of solvent evolution during the deposition process.

inward displacement ψ of the fluid in the resonator is

$$m'\ddot{\psi} + (R_r + R_\omega)\dot{\psi} + s_r\psi = S_a P_i \, \mathrm{e}^{\mathrm{i}\omega t}, \tag{2.7}$$

where a dot denotes a time derivative. Hence, the mechanical impedance of the resonator is given by

$$Z_m^r = R_r + R_\omega + \mathrm{i}\left(\omega m' - \frac{s_r}{\omega}\right), \tag{2.8}$$

where R_r, R_ω, m' and s_r are given by (2.1), (2.2), (2.4) and (2.6), respectively. In order to calculate this impedance, an expression for the volume of the resonator must be constructed. Considering the schematic of one resonator in Fig. 2, it can be seen that each cavity consists of a sphere with a 'removed cap' of base radius r_a and height h_a. The volume V_r of each resonator is then given by Weisstein (2013)

$$V_r = \frac{4}{3}\pi r_r^3 - \frac{\pi}{6}h_a(3r_a^2 + h_a^2), \tag{2.9}$$

where, by considering Pythagoras' theorem, h_a can be written in the form

$$h_a = r_r - \sqrt{r_r^2 - r_a^2}. \tag{2.10}$$

As mentioned, the backplate consists of an array of resonators. Consequently, each resonator's impedance must be combined to form a lumped acoustic impedance which can then be inserted into the model(s) for the displacement of the membrane. Defining $Z_m^r[i,j]$ as the mechanical impedance of the resonator in the ith row and jth column of the array of resonators, the specific acoustic impedance

of each resonator can then be given by $Z_s^r[i,j] = Z_m^r[i,j]/S_a[i,j]$ and the acoustic impedance of each resonator is given by $Z^r[i,j] = Z_m^r[i,j]/S_a^2[i,j]$. By summing the impedances of each resonator in each row of the array, and then summing the lumped impedances of each row, a form for the total impedance of the array of resonators can be found. That is, the sum of the impedances of each resonator in a row is given by

$$Z^r[j] = \frac{1}{\sum_{i=1}^{n_j} 1/Z^r[i,j]}, \tag{2.11}$$

where n_j is the number of resonators in row j. The sum of each row (the lumped acoustic impedance of the backplate, Z^b) is then calculated via

$$Z^b = \frac{1}{\sum_{j=1}^{N} 1/Z^r[j]}, \tag{2.12}$$

where N is the number of rows in the resonator array.

Consequently, given the dimensions of each resonator, and other associated parameters such as the speed of sound in the resonators, the lumped impedance of the backplate can be calculated and inserted into a model for the mechanical impedance of the device. The three models which describe the motion of the membrane, and consequently the mechanical impedance profile of the device, can now be illustrated.

2.2 *Model* I*: pipe-driver model*

This section considers the membrane as a pipe-driver system (see Kinsler *et al.*, 2000, p. 280). That is, the membrane is assumed to act like a damped harmonic oscillator, which is excited by an externally applied force $f(t)$. The displacement of the membrane ψ, from its equilibrium position, is given by

$$\begin{pmatrix}\text{mass of}\\ \text{membrane}\end{pmatrix}\begin{pmatrix}\text{membrane}\\ \text{acceleration}\end{pmatrix} + \begin{pmatrix}\text{viscous damping}\\ \text{in membrane}\end{pmatrix} + \begin{pmatrix}\text{drag forces}\\ \text{on membrane}\end{pmatrix} + \begin{pmatrix}\text{force from}\\ \text{excess pressure}\\ \text{in resonators}\end{pmatrix} + \begin{pmatrix}\text{driving}\\ \text{electrostatic}\\ \text{force}\end{pmatrix} = 0.$$

The viscous damping term is assumed to be proportional to the membrane velocity,

$$\text{viscous damping} = \frac{R_v}{S_m}\dot{\psi}, \tag{2.13}$$

where R_v is a damping constant and S_m is the surface area of the membrane. The drag forces on the membrane are also assumed to be proportional to the membrane velocity; however, the mechanical impedances of the adjacent fluids must be utilized,

$$\text{drag forces on membrane} = (Z_m^b + Z_m^l)\dot{\psi}. \tag{2.14}$$

Here, Z_m^b is the mechanical impedance of the backplate, related to the acoustic impedance given by (2.12), Z_m^l is the mechanical impedance of the fluid on the load side of the membrane, where the acoustic impedance of air is normally given as $413\,\text{Nsm}^{-3}$ at room temperature.

The excess pressure in the resonators is given by the percentage change in their volume as the membrane oscillates multiplied by the mechanical impedance of the fluid at the membrane–backplate

interface and the velocity of sound in the fluid. That is,

$$\text{excess pressure in resonators} = \frac{\Delta V_r}{V_r} Z_m^r c = \frac{S_a \psi}{V_r} Z_m^r c. \tag{2.15}$$

Care must be taken here concerning the spacing of the resonators. If each resonator is acting independently, that is, the resonators are sufficiently separated so that there is no coupling and each part of the membrane between the resonators has zero displacement (that is, it is clamped), then no summation of the resonators' volumes occurs. In this paper, it is assumed that the resonators are sufficiently spaced so that there is a zero displacement (Dirichlet) boundary condition around each resonator aperture perimeter.

The electrostatic force is given by Caronti *et al.* (2002)

$$F_e = \frac{CV^2}{2d_e^2}, \tag{2.16}$$

where $C = \epsilon_0 S_m / d_e$ is the capacitance of the device, ϵ_0 is the permittivity of free space, V is the applied voltage and d_e is the distance between the electrodes. It can be shown that the change in electrostatic force can be written as (see Caronti *et al.*, 2002; Walker & Mulholland, 2010)

$$\Delta F_E = \frac{\epsilon_0 S_m V_{\text{dc}}}{d_e^2} V_{\text{ac}} - \frac{\epsilon_0 S_m V_{\text{dc}}^2}{d_e^3} \psi, \tag{2.17}$$

where V_{dc} is the d.c. voltage and V_{ac} is the a.c. voltage. Hence, the dynamic equation for the membrane displacement is given by

$$d_m \rho_s \ddot{\psi} + \left(\frac{R_v}{S_m} + Z_s^l + \frac{S_a}{S_m} Z_s^b \right) \dot{\psi} + \left(\frac{S_a Z_m^r c}{S_m V_r} - \frac{\epsilon_0 V_{\text{dc}}^2}{d_e^3} \right) \psi = f(t), \tag{2.18}$$

where d_m is the thickness of the membrane, ρ_s is the density of the membrane, Z_s^l is the specific acoustic impedance of the fluid at the load side of the membrane and the space between the electrodes d_e is given by

$$d_e = \frac{d_m}{\epsilon_r} + L_m + x_{\text{dc}}, \tag{2.19}$$

where ϵ_r is the relative permittivity of the membrane, L_m is the distance between the inner surface of the membrane and the lower electrode, x_{dc} is the displacement of the membrane due to a bias d.c. voltage V_{dc} and $f(t)$ is the voltage driving force applied to the membrane given by

$$f(t) = \frac{\epsilon_0 V_{\text{dc}} V_{\text{ac}}(t)}{d_e^2}. \tag{2.20}$$

Taking the Fourier transform (see Wright, 2005) of equation (2.18) gives

$$\left[-\omega^2 d_m \rho_s + \mathrm{i}\omega \left(\frac{R_v}{S_m} + Z_s^l + \frac{S_a}{S_m} Z_s^b \right) + \left(\frac{S_a Z_m^r c}{S_m V_r} - \frac{\epsilon_0 V_{\text{dc}}^2}{d_e^3} \right) \right] \Psi = F, \tag{2.21}$$

where Ψ is the membrane displacement in the frequency domain and F is the voltage driving force in the frequency domain. The frequency domain response of the system is then

$$\Psi = \frac{F}{\mathrm{i}\omega Z_s^{\mathrm{I}}}, \tag{2.22}$$

where Z_s^{I} is the combined specific acoustic impedance of the system given by

$$Z_s^{\mathrm{I}} = \mathrm{i}\omega d_m \rho_s + \left(\frac{R_v}{S_m} + Z_s^l + \frac{S_a}{S_m} Z_s^b\right) - \frac{\mathrm{i}}{w}\left(\frac{S_a Z_m^r c}{S_m V_r} - \frac{\epsilon_0 V_{\mathrm{dc}}^2}{d_e^3}\right), \tag{2.23}$$

and

$$F = \frac{\epsilon_0 V_{\mathrm{dc}} \bar{V}_{\mathrm{ac}}(\omega)}{d_e^2}, \tag{2.24}$$

where $\bar{V}_{\mathrm{ac}}(\omega)$ is the Fourier transform of the a.c. voltage $V_{\mathrm{ac}}(t)$. Consequently, the velocity of the membrane is the frequency domain is

$$\dot{\Psi} = \frac{1}{Z_s^{\mathrm{I}}} F. \tag{2.25}$$

Hence, the amplitude of the pressure produced at the membrane–fluid load interface is

$$P_o = \dot{\Psi} Z_s^l. \tag{2.26}$$

The device outputs of interest are the mechanical impedance, and the transmission and reception sensitivities. The transmission and reception sensitivities are calculated in the same manner for each model in Section 2.5.

2.3 *Model* II*: membrane model*

In this section the analysis to describe the membrane is provided, following a similar methodology to that by Caronti *et al.* (2002). Assuming that the Mylar membrane is thin and the dominant restoring force comes from the tension in the membrane, the membrane equation can be used to model the displacement of the Mylar membrane. It is given by

$$\nabla^2 \psi(r,\omega) + A_m^2 \psi(r,\omega) = B_m + C_m \int_0^{r_a} r\psi(r,\omega)\,\mathrm{d}r, \tag{2.27}$$

where $\psi(r,\omega)$ is the displacement of the membrane at any point in its radius $r \leqslant r_a$ and frequency ω, and A_m^2 accounts for viscous damping forces arising from the energy losses of the vibrating membrane and the impedance arising from the design in the backplate, given by

$$A_m^2 = -\frac{1}{\tau}\left(-\omega^2 d_m \rho_s + \mathrm{i}\omega\left(\frac{R_v}{S_m} + Z_s^l + \frac{S_a}{S_m} Z_s^b\right) + \left(\frac{S_a Z_m^r c}{S_m V_r} - \frac{\epsilon_0 V_{\mathrm{dc}}^2}{d_e^3}\right)\right), \tag{2.28}$$

where τ is the tensile stress per unit length. The constant B_m takes into account the excitation voltage and is given by

$$B_m = \frac{\epsilon_0 V_{\mathrm{dc}} V_{\mathrm{ac}}(t)}{\tau d_e^2}, \tag{2.29}$$

and C_m is related to the average displacement of the membrane and is given by

$$C_m = \frac{2\rho_a c^2}{\tau r_r^2 L_m}. \tag{2.30}$$

The homogeneous part of equation (2.27) is in the form of Bessel's equation and hence the complementary function is given by

$$\psi_{cf}(r,\omega) = C_1 J_0(\lambda_m r) + C_2 Y_0(\lambda_m r), \tag{2.31}$$

where C_1, C_2 and λ_m are all functions of ω to be found and J_0 and Y_0 are the Bessel functions of the first and second kind of zero order (see Sneddon, 1980). Since the displacement of the membrane must exist at $r = 0$ (the centre of the membrane) then $C_2 \equiv 0$ since $Y_0(\lambda_m r) \to \infty$ as $r \to 0$. Inserting the complementary function into the auxiliary solution enables us to show that $\lambda_m = A_m$ and thus a particular integral of the from

$$\psi_{pi}(r,\omega) = C_1 J_0(A_m r) + C_3, \tag{2.32}$$

should be chosen, where C_3 is an arbitrary function of ω to be solved for. Inserting the particular integral (2.32) into the integro-differential equation (2.27) provides us with the solution for the function C_2, namely

$$C_2 = \bar{B}_m + C_1 \bar{C}_m, \tag{2.33}$$

where

$$\bar{B}_m = \frac{B_m}{(A_m^2 - (1/2)C_m r_a^2)} \quad \text{and} \quad \bar{C}_m = \frac{C_m r_a J_1(A_m r_a)}{A_m(A_m^2 - (1/2)C_m r_a^2)}, \tag{2.34}$$

with J_1 being the Bessel function of the first kind of first order (see Sneddon, 1980). Since the displacement of the membrane is zero apart from where it sits directly above the resonator aperture then the appropriate boundary condition is $\psi(r_a, 0) = 0$, and hence C_1 is given by

$$C_1 = -\frac{\bar{B}_m}{J_0(A_m r_a) + \bar{C}_m}. \tag{2.35}$$

Consequently, the full solution to the membrane equation (2.27) is given by

$$\psi(r,\omega) = -\frac{\bar{B}_m}{(J_0(A_m r_a) + \bar{C}_m)} J_0(A_m r) + \bar{B}_m - \frac{\bar{B}_m \bar{C}_m}{(J_0(A_m r_a) + \bar{C}_m)}. \tag{2.36}$$

The velocity of the membrane and, in turn, the impedance of the system, can then be given via the spatially averaged displacement $\langle\psi\rangle$, given by Caronti *et al.* (2002)

$$\langle\psi\rangle = \frac{1}{\pi r_a^2} \int_0^{r_a} \psi(r,\omega) 2\pi r \, \mathrm{d}r. \tag{2.37}$$

The specific acoustic impedance is defined as the ratio of the driving electrostatic force and the product of the average velocity of the membrane and its surface area. Consequently, it can be written

$$Z_s^{\mathrm{II}}(\omega) = \frac{C_m A_m}{\mathrm{i}\omega(-2(\bar{B}_m/(J_0(A_m r_a) + \bar{C}_m))J_1(A_m r_a) + A_m r_a \bar{B}_m A_m r_a (\bar{B}_m \bar{C}_m/(J_0(A_m r_a) + \bar{C}_m)))}. \tag{2.38}$$

This impedance will be used in the following section to provide a comparison with the other two models.

2.4 *Model* III*: plate model*

In this section the analysis for the plate model is provided. That is, it is assumed that the dominant contribution to the restoring force of the membrane comes from its stiffness. Consequently, plate theory is applied to model the membrane. The equation of motion for symmetric harmonic vibrations can be constructed via (Caronti *et al.*, 2002)

$$\nabla^4\psi(r,\omega) - A_p^4\psi(r,\omega) = B_p - C_p\int_0^{r_a}\psi(r,\omega)r\,\mathrm{d}r, \tag{2.39}$$

where $\psi(r,\omega)$ is the displacement of the membrane at any point in its radius r and frequency ω, and A_p^4 accounts for viscous damping forces arising from the energy losses of the vibrating membrane and the impedance arising from the design in the backplate, given by

$$A_p^4 = -\frac{1}{D}\left(-\omega^2 d_m\rho_s + \mathrm{i}\omega\left(\frac{R_v}{S_m} + Z_s^l + \frac{S_a}{S_m}Z_s^b\right) + \left(\frac{S_a Z_m^r c}{S_m V_r} - \frac{\epsilon_0 V_{\mathrm{dc}}^2}{d_e^3}\right)\right), \tag{2.40}$$

where D is the flexural rigidity of the membrane. The function B_p takes into account the excitation voltage and is given by

$$B_p = \frac{\epsilon_0 V_{\mathrm{dc}} V_{\mathrm{ac}}(t)}{D(d_m/\epsilon_r + L_m)^3}, \tag{2.41}$$

and C_p is related to the average displacement of the membrane, with C_p being given by

$$C_p = \frac{2\rho_a c^2}{Dr_r^2 L_m}. \tag{2.42}$$

The solution to the homogeneous part of equation (2.39) is given by

$$\psi_{cf}(r) = C_4 J_0(A_p r) + C_5 Y_0(A_p r) + C_6 J_0(\mathrm{i}A_p r) + C_7 Y_0(\mathrm{i}A_p r), \tag{2.43}$$

where C_4, C_5, C_6 and C_7 are functions of ω to be solved for. Since the solution must exist at $r \equiv 0$ (at the centre of the membrane) then $C_5 \equiv C_7 \equiv 0$ and recalling $J_0(\mathrm{i}x) \equiv I_0(x)$ (see Watson, 1996, p. 77), where I_0 is the modified Bessel function of the first kind of order zero, a particular integral of the form

$$\psi_{pi}(r,\omega) = C_4 J_0(A_p r) + C_6 I_0(A_p r) + C_8, \tag{2.44}$$

can be assumed. Inserting this into the integro-differential equation (2.39) provides us with the solution for C_8, namely

$$C_8 = \bar{B}_p + C_4\bar{C}_p J_1(A_p r_a) + C_6\bar{C}_p I_1(A_p r_a), \tag{2.45}$$

where

$$\bar{B}_p = -\frac{B_p}{A_p - (1/2)C_p r_a^2}, \quad \bar{C}_p = \frac{C_p r_a}{A_p(A_p - (1/2)C_p r_a^2)}. \tag{2.46}$$

Similar to the previous model, we assume that the membrane has zero displacement outwith the support of the resonator aperture and so $\psi(r_a,\omega) = 0$. Here we also require a condition on the spatial derivative on the perimeter of the aperture and so we set $\psi'(r_a,\omega) = 0$. This condition concurs with the assumption

that the membrane has zero displacement, and hence zero velocity, outwith the support of the resonator. Hence, two equations to solve for our two remaining unknowns C_4 and C_6 are provided and we find

$$C_4 = -\frac{\bar{B}_p I_1(A_p r_a)}{\hat{B}_p}, \quad C_6 = -\frac{\bar{B}_p J_1(A_p r_a)}{\hat{B}_p}, \tag{2.47}$$

where

$$\hat{B}_p = J_0(A_p r_a) I_1(A_p r_a) + 2\bar{C}_p J_1(A_p r_a) I_1(A_p r_a) + J_1(A_p r_a) I_0(A_p r_a). \tag{2.48}$$

Consequently, the full solution to the plate equation (2.39) is given by

$$\begin{aligned}\psi(r,\omega) = &-\frac{\bar{B}_p I_1(A_p r_a)}{\hat{B}_p} J_0(A_p r) - \frac{\bar{B}_p J_1(A_p r_a)}{\hat{B}_p} I_0(A_p r) + \bar{B}_p \\ &- \frac{\bar{B}_p I_1(A_p r_a)}{\hat{B}_p} \bar{C}_p J_1(A_p r_a) - \frac{\bar{B}_p J_1(A_p r_a)}{\hat{B}_p} \bar{C}_p I_1(A_p r_a).\end{aligned} \tag{2.49}$$

As in the previous section, the specific acoustic impedance is the ratio of the driving electrostatic force and the product of the average velocity over the surface of the membrane and the membrane's surface area, given by

$$Z_s^{\mathrm{III}} = \frac{B_p \pi r_a^2}{\mathrm{i}\omega \langle \psi \rangle S_m}, \tag{2.50}$$

where $\langle \psi \rangle$ is the average mechanical behaviour of the membrane, defined similarly to equation (2.37). The full formulation of this impedance is omitted for brevity.

2.5 *Electrical impedance, transmission and reception sensitivities of the device*

A transducer converting electrical and mechanical energy forms a two-port network that relates electrical quantities at one port to mechanical quantities at the other (see Kinsler *et al.*, 2000, p. 390). The canonical equations which describe this are given by

$$\bar{V}_{\mathrm{ac}} = Z_{\mathrm{EB}} I + T\dot{\Psi}, \tag{2.51}$$

$$F = TI + Z_{\mathrm{mo}}\dot{\Psi}, \tag{2.52}$$

where $\dot{\Psi}$ is the velocity of the membrane, calculated from any of the three previous models, I is the current at the electrical inputs, F is the force on/from the radiating surface, Z_{EB} is the blocked electrical impedance ($\dot{\Psi} = 0$), Z_{mo} is the open-circuit mechanical impedance ($I = 0$) and T is the transduction coefficient (mechanical $\leftrightarrow$ electrical). In the short circuit case $\bar{V}_{\mathrm{ac}} = 0$ it can be shown

$$\frac{F}{\dot{\Psi}} = \left(Z_{\mathrm{mo}} - \frac{T^2}{Z_{\mathrm{EB}}} \right) = Z_m, \tag{2.53}$$

where Z_m is the mechanical impedance of the transducer. Hence equations (2.51) and (2.52) can be rewritten as

$$\bar{V}_{\mathrm{ac}} = Z_{\mathrm{EB}} I + \beta Z_{\mathrm{EB}}\dot{\Psi}, \tag{2.54}$$

$$F = \beta Z_{\mathrm{EB}} I + Z_m \dot{\Psi}, \tag{2.55}$$

respectively, where the transformation factor β is given by $\beta = T/Z_{\mathrm{EB}}$. When the source (a.c.) voltage is of the form $V_{\mathrm{ac}}(t) = V_{\mathrm{ac}}\,\mathrm{e}^{\mathrm{i}\omega t}$, then by Caronti *et al.* (2002), Kinsler *et al.* (2000) and Walker & Mulholland (2010)

$$V_{\mathrm{ac}} = \left(\frac{1}{G + \mathrm{i}\omega C_0}\right) I + \frac{V_{dc}}{\mathrm{i}\omega x_{\mathrm{dc}}}\dot{\Psi}, \tag{2.56}$$

where G is the static conductance caused by electrical losses in the device and C_0 is the value of C at $\dot{\Psi} = 0$. Hence, comparing with equations (2.51) and (2.52) the transformation factor β can be given as (see Walker & Mulholland, 2010)

$$\beta = \frac{V_{\mathrm{dc}} C_0}{x_{\mathrm{dc}}} - \mathrm{i}\frac{G V_{\mathrm{dc}}}{\omega x_{\mathrm{dc}}}, \tag{2.57}$$

where $C_0 = \epsilon_0 S_m/(d_m/\epsilon_r + L + x_{\mathrm{dc}})$. Consequently, the blocked electrical impedance is given by

$$Z_{\mathrm{EB}} = \frac{1}{G + \mathrm{i}\omega C_0}. \tag{2.58}$$

2.5.1 *Transmission sensitivity* In transmission mode, a voltage $\bar{V}_{\mathrm{ac}}$ is applied that results in a membrane velocity $\dot{\Psi}$ and hence a force F being produced, where

$$F = -Z_m \dot{\Psi}. \tag{2.59}$$

The transmission sensitivity, or TVR, is defined here as the ratio of the transmitted pressure to the driving voltage (see Caronti *et al.*, 2002). That is

$$\mathrm{TVR} = \frac{P_o S_m}{V_{\mathrm{ac}}}. \tag{2.60}$$

After some algebraic manipulation, it can be shown that (via Walker & Mulholland, 2010)

$$\mathrm{TVR} = -\frac{\beta}{(1 + Z_m^b/Z_m)}. \tag{2.61}$$

This can now be evaluated using equations (2.57) and the various equations for the mechanical impedance of the transducer Z_m and the mechanical impedance of the backplate Z_m^b.

2.5.2 *Reception sensitivity* The reception sensitivity is defined as the ratio of the open-circuit ($I = 0$) output voltage to the force on the membrane (see Caronti *et al.*, 2002). That is, the RFR is given by

$$\mathrm{RFR} = \frac{\bar{V}_{\mathrm{ac}}}{P_o S_m}. \tag{2.62}$$

Setting $I = 0$ (for the open-circuit) in equations (2.51) and (2.52) gives

$$\bar{V}_{\mathrm{ac}} = T\dot{\Psi}, \tag{2.63}$$

$$F = Z_{\mathrm{mo}}\dot{\Psi}. \tag{2.64}$$

Since $F = P_o S_m$ then $\dot{\Psi} = P_o S_m / Z_{\text{mo}}$ and so from equation (2.63) it can be shown that

$$\bar{V}_{\text{ac}} = \frac{Z_{\text{EB}} \beta P_o S_m}{Z_{\text{mo}}}.$$

Inserting this formulation for the voltage into equation (2.62) gives

$$\text{RFR} = \beta \frac{Z_{\text{EB}}}{Z_{\text{mo}}}. \tag{2.65}$$

It can also be shown that $Z_{\text{mo}} = Z_m + T^2 / Z_{\text{EB}}$ and hence equation (2.65) can be written

$$\text{RFR} = \frac{\psi Z_{\text{EB}}}{Z_m + (T^2 / Z_{\text{EB}})}. \tag{2.66}$$

Again this can be evaluated via equations (2.57) and (2.58) and the equations given for the mechanical impedance in each model.

The three models are now compared, by investigating the mechanical impedance, the TVR and the RFR in the next section.

3. Comparison of models

In this section a comparison between the three models presented in the previous sections is provided. Of particular interest is the operating frequency of the devices since the resonators are included in order to tailor the devices to a specific frequency. Consequently, this section provides plots of the impedance profiles from the backplate and the entire system, in addition to the TVR and RFR.

In order to successfully compare the three models, material and design parameter values must be considered. Initial endeavours in manufacturing backplates have taken place and form the basis for the backplate design parameter values given in Table 1. Additional design and material parameter values are given in Table 2.

As mentioned previously, the resonators must be sufficiently spaced such that no coupling between each resonator occurs. Within the model the parameters N and n_j (the number of rows of resonators and the number of resonators in each row) can be adjusted to examine the effect of this spacing on the device performance. Here we will simply choose a number of resonators that is commensurate with those used in preliminary experiments.

The mechanical impedance profiles of the resonators are then computed via the equations provided in Section 2.1. For the design parameter values given in Tables 1 and 2, the normalized mechanical

TABLE 1 *Design values of the backplate and the spherical resonators therein*

Design parameter	Symbol	Magnitude	Dimensions
Radius of resonators	r_r	25	μm
Radius of apertures/membrane	r_a	20	μm
Thickness of backplate	L_m	1	mm

TABLE 2 *Parameter and design values of the transducer*

Design parameter	Symbol	Magnitude	Dimensions
Speed of sound in air	c	343	m/s
Density of air in resonator	ρ_a	1.2	kg/m^3
Attenuation coefficient	γ_ω	0.001	—
Thickness of membrane	d_m	8	μm
Membrane dielectric constant	ϵ_r	5	—
Coefficient of shear viscosity	η	1.78	Pa s
Prandtl number	Pr	0.75	—
d.c. Voltage	V_{dc}	200	V
Applied voltage	V	200	V
Density of mylar membrane	ρ_s	1420	kg/m^3
d.c. Deflection on membrane	x_{dc}	60	nm
Permittivity of free space	ϵ_0	8.85×10^{-12}	F/m
Damping coefficient	R_v	100	kg/m s

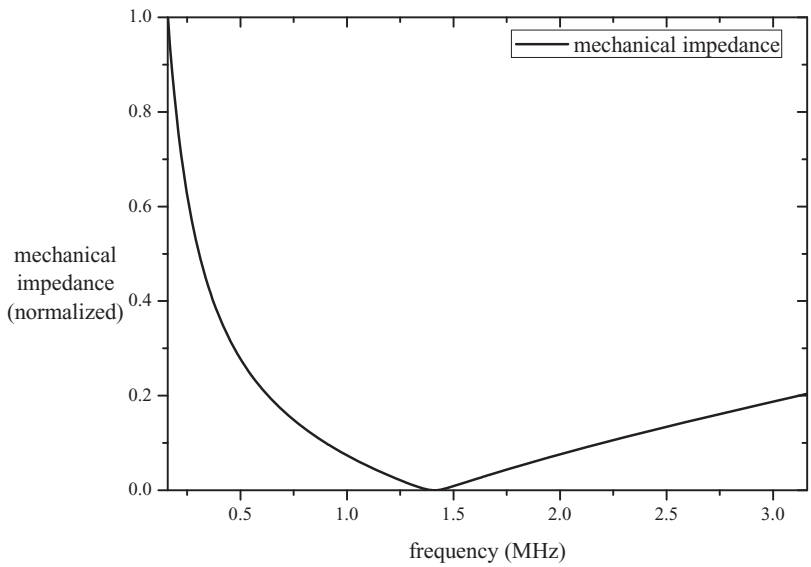

FIG. 3. Normalized mechanical impedance of the array of resonators with dimensions provided in Table 1. Note the impedance minimum, and hence system resonance at approximately 1.5 MHz.

impedance of the resonator array is shown in Fig. 3. It is clearly seen that the minimum impedance occurs around 1.5 MHz and therefore a central operating frequency of the device around this frequency is expected.

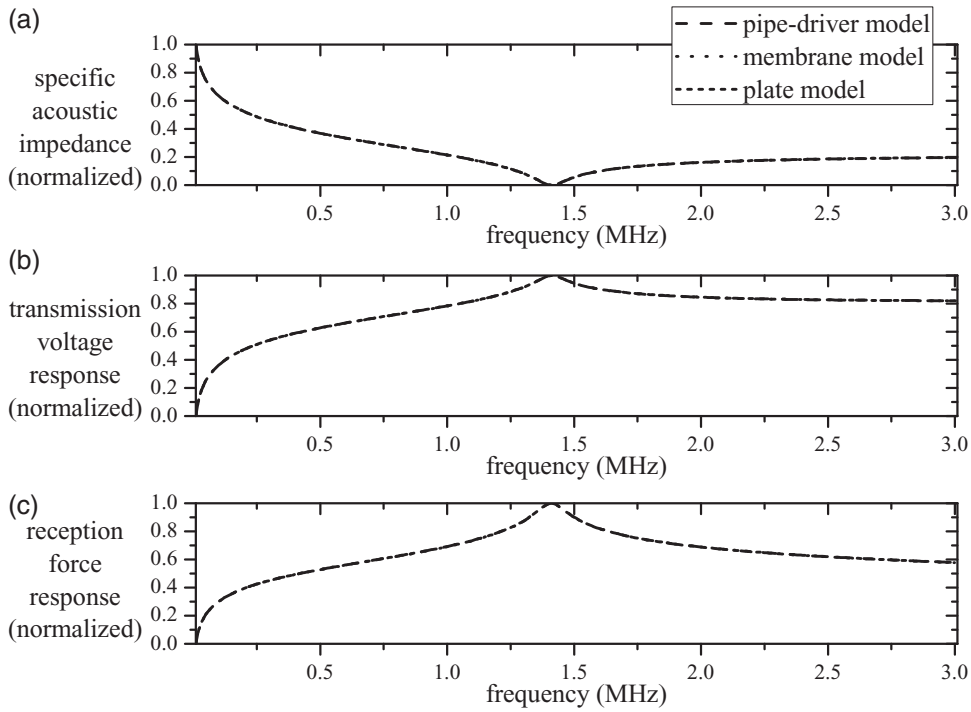

FIG. 4. Normalized specific acoustic impedance (a), normalized TVR (b) and normalized RFR (c) of the three models. The pipe-driver model is dashed, the membrane model is dotted and the plate model is short dashed. The three lines lie on top of each other and illustrate the excellent corroboration between each model.

For comparison purposes the specific acoustic impedance of each model is normalized with respect to its maximum value achieved and then expressed in decibels via

$$\hat{Z}_s^{\mathrm{I}} = 20\log_{10}\left(\frac{Z_s^{\mathrm{I}}}{\max(Z_s^{\mathrm{I}})}\right), \tag{3.1}$$

$$\hat{Z}_s^{\mathrm{II}} = 20\log_{10}\left(\frac{Z_s^{\mathrm{II}}}{\max(Z_s^{\mathrm{II}})}\right), \tag{3.2}$$

$$\hat{Z}_s^{\mathrm{III}} = 20\log_{10}\left(\frac{Z_s^{\mathrm{III}}}{\max(Z_s^{\mathrm{III}})}\right), \tag{3.3}$$

where $\hat{Z}_s^{\mathrm{I}}$, $\hat{Z}_s^{\mathrm{II}}$ and $\hat{Z}_s^{\mathrm{III}}$ are the normalized specific acoustic impedances in decibels of the pipe-driver model, the membrane model and the plate model, respectively.

The normalized specific acoustic impedance of the device for each model, given by equations (2.23), (2.38) and (2.50), is shown in Fig. 4(a). It is clear to see that there is excellent corroboration between each model. This fact suggests that any of the three models here could be used in order to model this device as well as other similar devices. Furthermore, it suggests that the effects of the resonators far outweigh those of the membrane's stiffness or rigidity. In a similar manner to the specific acoustic

impedances, the normalized TVR and the normalized RFR are calculated, in decibels, for each model. These are given by, respectively,

$$\widehat{\mathrm{TVR}} = 20\log_{10}\left(\frac{\mathrm{TVR}}{\max(\mathrm{TVR})}\right), \tag{3.4}$$

$$\widehat{\mathrm{RFR}} = 20\log_{10}\left(\frac{\mathrm{RFR}}{\max(\mathrm{RFR})}\right). \tag{3.5}$$

The TVR for all models is given in Fig. 4(b) and the RFR in Fig. 4(c). It is clear that all models closely agree for both the TVR and the RFR.

Since the three models corroborate, the effect of changing some of the parameters of the resonators on the outputs of the device is examined. Specifically, the changes in the TVR and the RFR are considered.

4. Influence of design parameters

In this section the dependence on certain design parameters related to the spherical resonators are considered. As the outputs of the three models closely match, we inspect only the pipe-driver model described in Section 2.2. Three separate investigations were implemented. The parameters varied were the aperture size (with corresponding scaled resonator volume), the aperture size (with fixed resonator volume) and the neck length (where the neck length was equal to zero in the standard case). It should be noted first of all that all of the above investigations revealed no change in the electrical impedance of the system, as expected.

4.1 *Aperture and resonator size*

The case where the aperture size is varied, with the ratio between aperture radius and resonator radius kept constant, is considered. Primarily, five different values of the aperture radius are considered: $r_a = 1\,\mathrm{nm}$ (solid line), 10 nm (dashed line), 100 nm (dotted line), $1\,\mu\mathrm{m}$ (dash dot line) and $25\,\mu\mathrm{m}$ (dash dot dot line). The last value being the largest aperture size possible since $r_r = 25\,\mu\mathrm{m}$, as per Table 1. The first value of $r_a = 1\,\mathrm{nm}$ should give an indication of how a similar device with no resonators would operate. Figure 5(a) shows the TVR for these five different designs with it being clearly illustrated that the inclusion of resonators with larger apertures (and corresponding larger volumes) results in a higher TVR and a more prominent resonant frequency, although perhaps a reduced bandwidth. By considering the normalized TVR (Fig. 5(b)) it can be seen that the resonant frequency varies substantially from a sub-ultrasonic resonance ($r_a = 1\,\mu\mathrm{m}$, dash-dot) to resonances in the range of $5 - 7\,\mathrm{MHz}$. Since there is clearly a high dependence on the aperture radius, it was decided to investigate the dependence of the TVR on the aperture radius for a fixed frequency of $f = 1\,\mathrm{MHz}$. This dependence can be found in Fig. 5(c). The figure clearly shows that the TVR is maximized by a value of $r_a \approx 12\,\mu\mathrm{m}$.

The RFR follows a similar pattern in all but the resonant frequency positions. Using the same variables as in the TVR case, the results are shown in Fig. 6. The results suggest that the device operates in a similar frequency range in the reception and transmission modes; however, it does appear that the device operates substantially better in the reception mode. By varying the aperture size, it seems that the RFR is maximized by a design parameter choice of $r_a \approx 12\,\mu\mathrm{m}$. It is also seen that the larger the

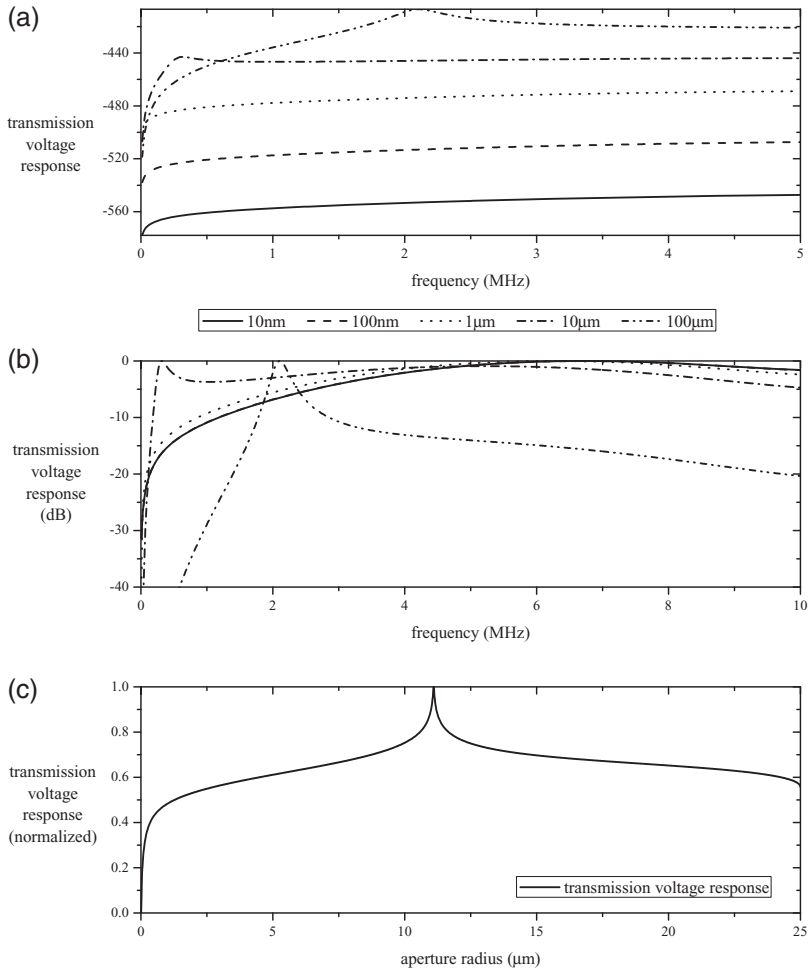

FIG. 5. TVR (a) and normalized transmission voltage response in dB (b) of the device, for each of the five values for the aperture radius (with corresponding resonator volume). Normalized TVR as a function of aperture radius for fixed frequency $f = 1$ MHz (c).

aperture size, the higher the resonant frequency of the device. However, it should be noted that only the largest aperture size results in an RFR in the ultrasonic range.

4.2 *Aperture size with fixed resonator volume*

The effect of changing the aperture size, where the volume of the whole resonator is kept constant, is now considered. For ease of comparison, the aperture sizes considered are the same as in the previous section, whereas the volume of the resonator is kept at the same size as in the standard design (calculated via equation (2.9) and Table 1). This is clearly not attainable using the chemical set-up described in the introduction to the article, but instead is an interesting mathematical investigation into how the nature of the resonators affects the device's performance.

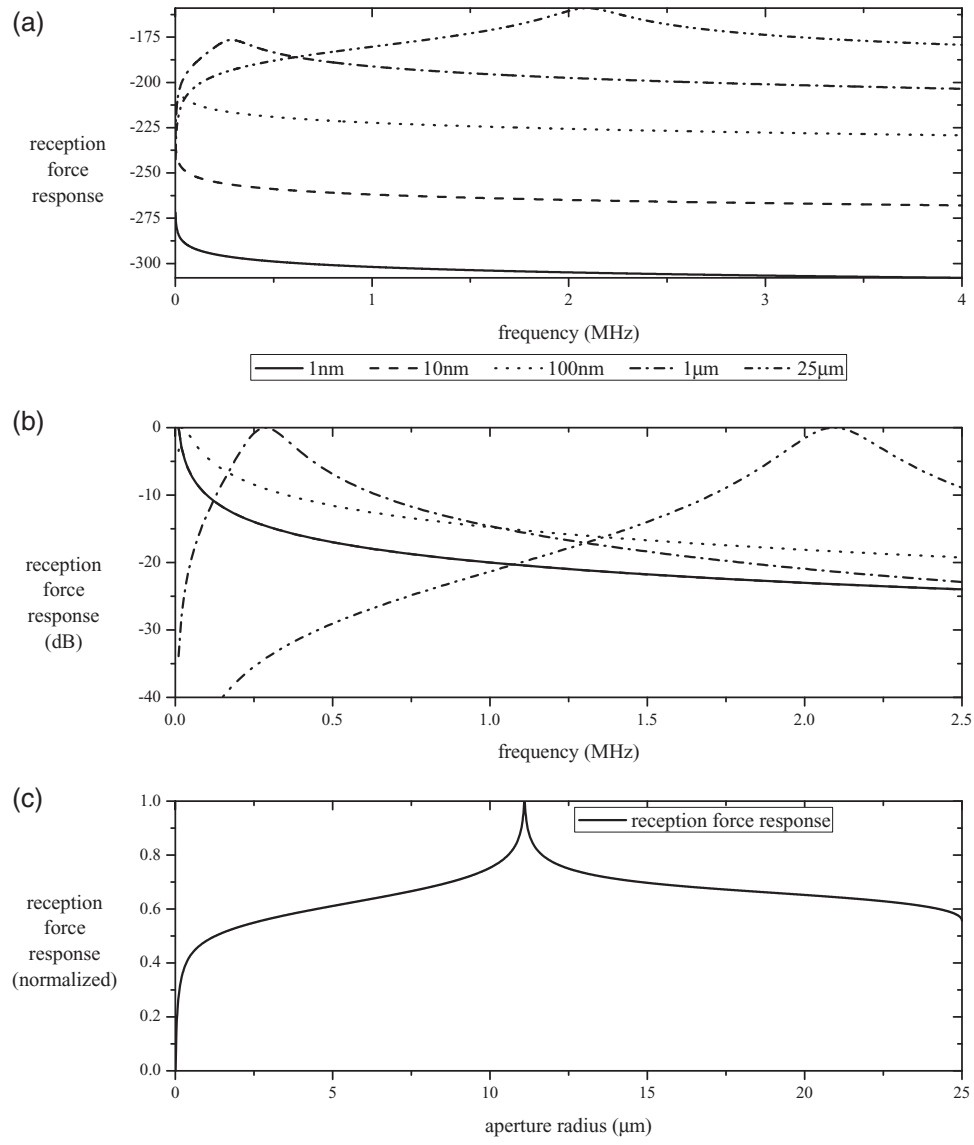

FIG. 6. RFR (a) and normalized RFR in dB (b) of the device, for each of the five values for the aperture radius (with corresponding resonator volume). Normalized RFR as a function of aperture radius for fixed frequency $f = 1$ MHz (c).

The TVR, normalized TVR and effect of aperture radius for a fixed frequency are given by Fig. 7. As can be seen, there are no large differences between these results and those in the previous section, save for the value of $r_a \approx 10\,\mu$m which maximizes the TVR. The same can be said for the RFR, normalized RFR and the effect of aperture radius, given by Fig. 8. Both sets of devices operate in the same range of frequencies and both follow similar responses when varying the aperture size. It can therefore be concluded that it is the aperture size which has more influence on the operation of the device than the volume of the resonators.

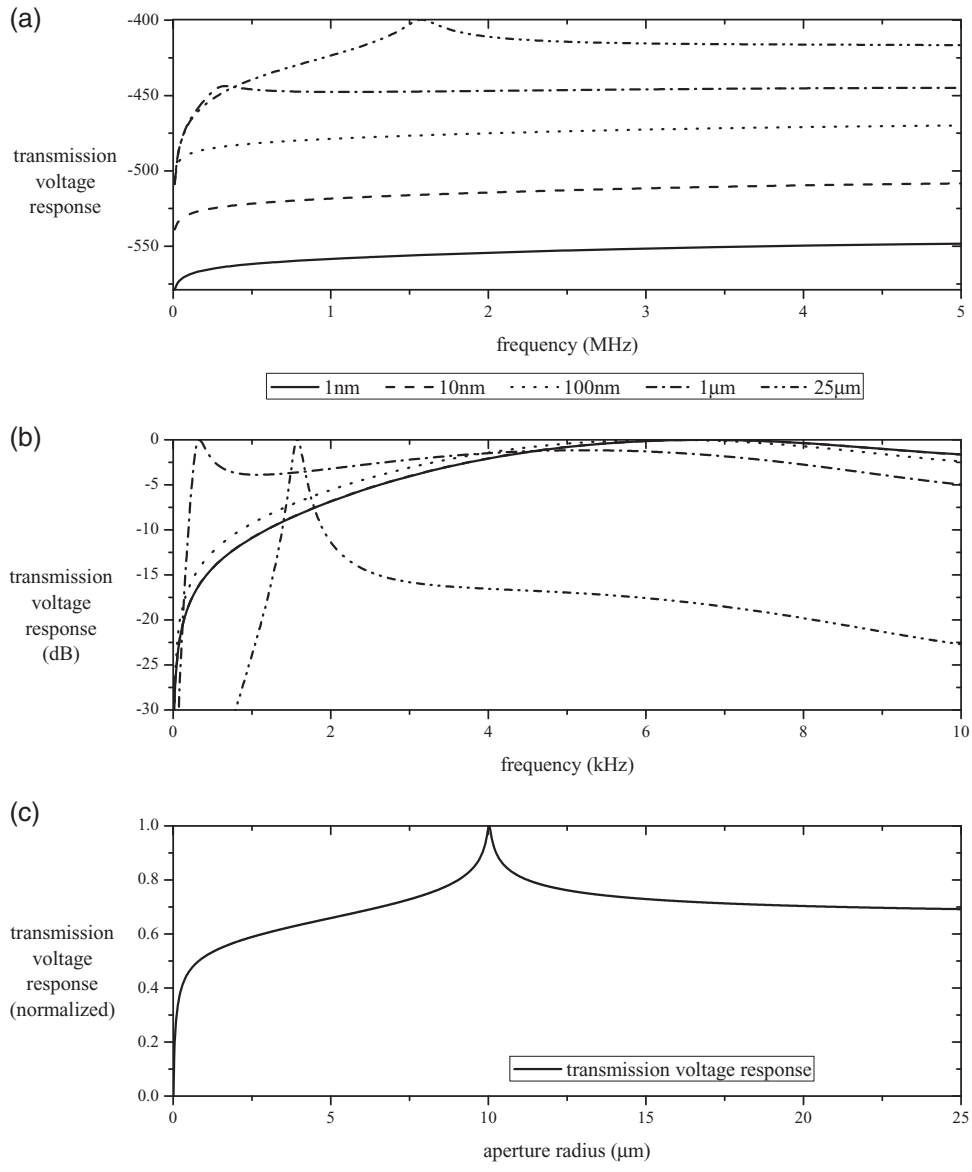

FIG. 7. TVR (a) and normalized transmission voltage response in dB (b) of the device, for each of the five values for the aperture radius (with fixed resonator volume). Normalized TVR as a function of aperture radius for fixed frequency $f = 1$ MHz (c).

4.3 *Neck length*

Finally the effect of constructing a neck on the resonator is scrutinized in order to investigate a possible change in the design which results in an improved bandwidth or resonating frequency. That is, it is not assumed that $L = 0$ in equation (2.5). To begin, five different lengths of the neck are chosen: $L = 0$ m (solid line), 1 μm (dashed line), 10 μm (dotted line), 100 μm (dash-dot line) and 1 mm (dash-dot-dot line). The TVR and normalized TVR are shown via Fig. 9(a,b). These figures show the dependence

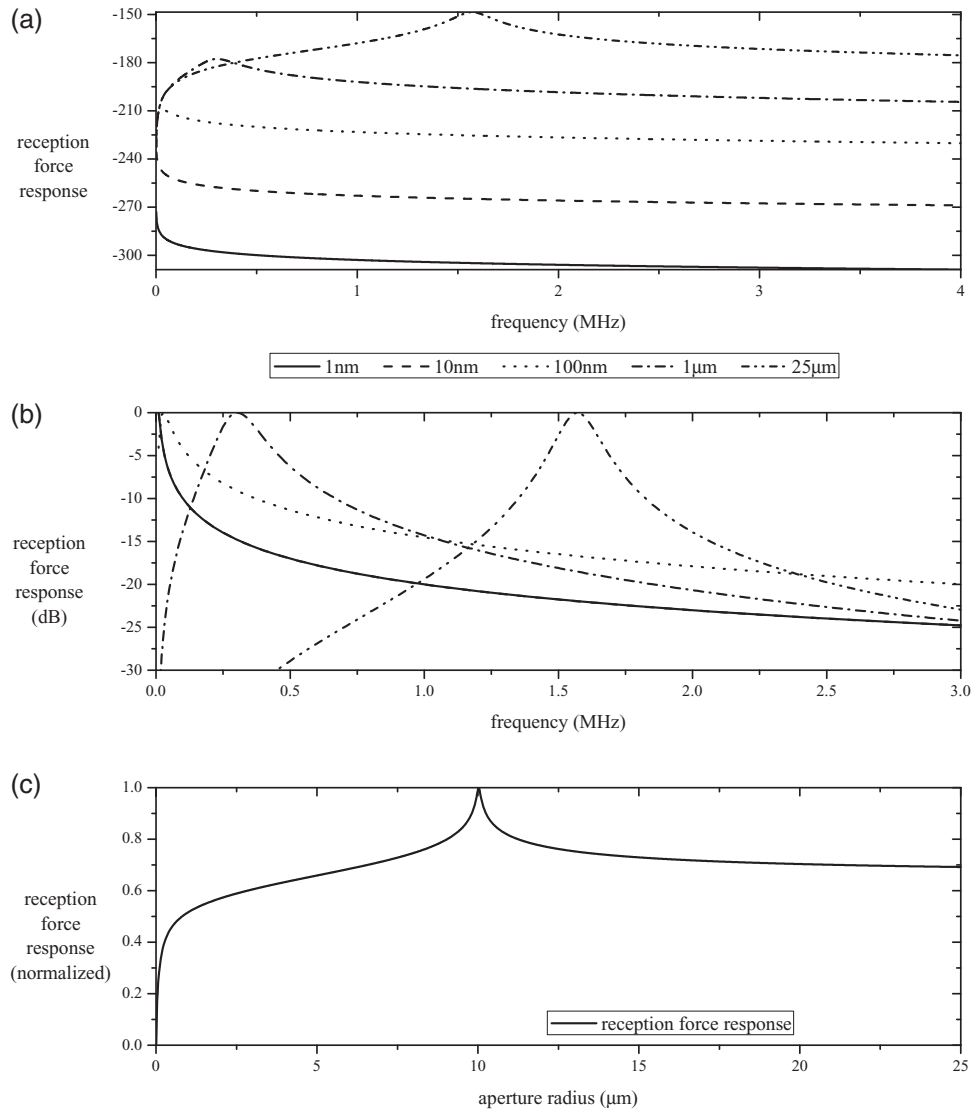

FIG. 8. RFR (a) and normalized RFR in dB (b) of the device, for each of the five values for the aperture radius (with fixed resonator volume). Normalized RFR as a function of aperture radius for fixed frequency $f = 1$ MHz (c).

of the magnitude, bandwidth and resonating frequency of the device on the length of the neck. It can be seen that the longer the neck, the narrower the bandwidth and the lower the resulting resonating frequency. Figure 9(a) also suggests that the highest TVR occurs when the length of the neck is between 10 and 100 μm. The actual value of this can be seen easier in Fig. 9(c), where the TVR is plotted against the effective length for $f = 1$ MHz. Note that $L \approx 32\,\mu$m gives the best TVR. A similar analysis was done for the RFR. Figure 10 shows the same effect of the resonator neck length on the RFR as the TVR.

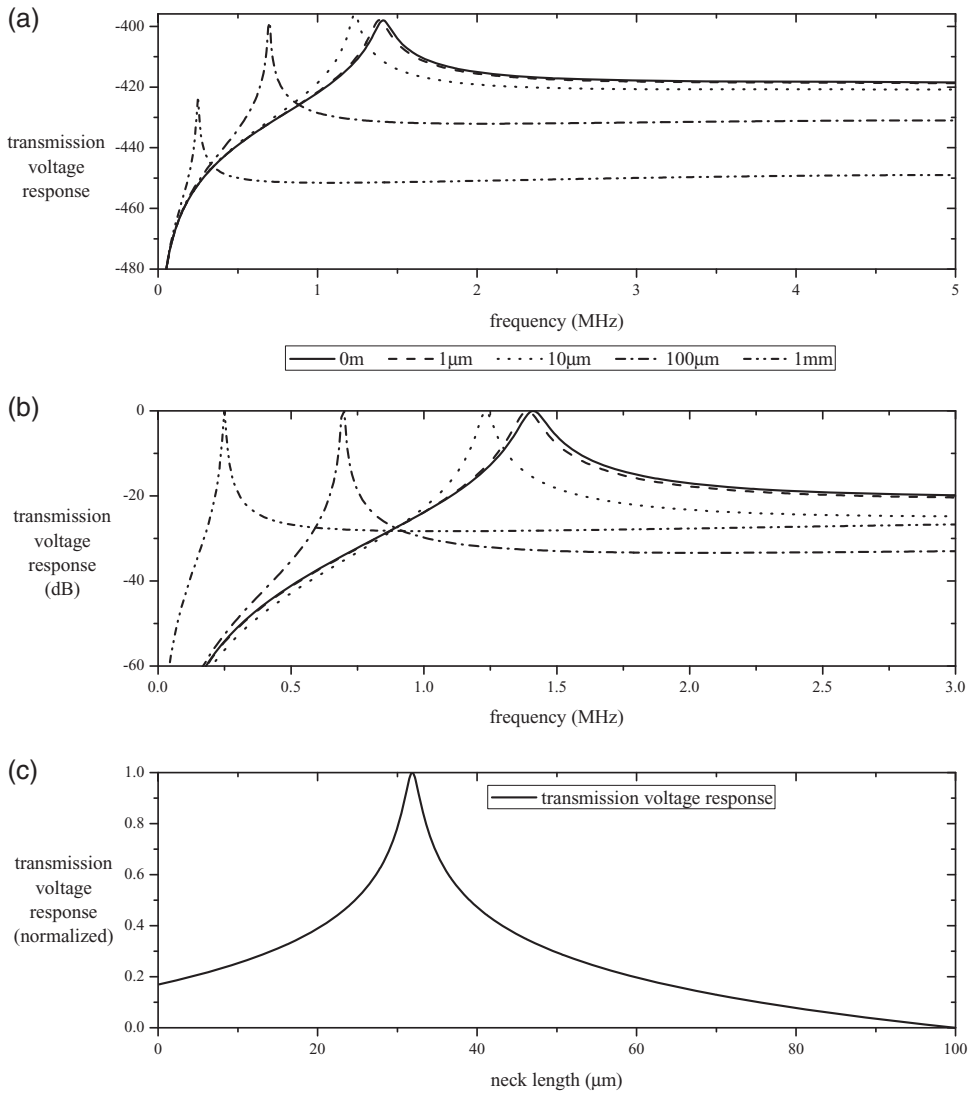

FIG. 9. TVR (a) and normalized transmission voltage response in dB (b) of the device, for each of the five values for the neck length. Normalized TVR as a function of the neck length for fixed frequency $f = 1$ MHz (c).

5. Conclusions and discussion

This article considered the theoretical modelling of a novel electrostatic transducer in which the backplate consisted of an array of spherical resonators which act in a similar manner to cavities/pits found in more standard devices. The resonators are made by depositing ternary solutions onto an electrically conducting substrate and the spherical resonators can be created by selective dissolution of one polymer phase after phase separation. The dimensions of the cavities and their spatial distribution can be

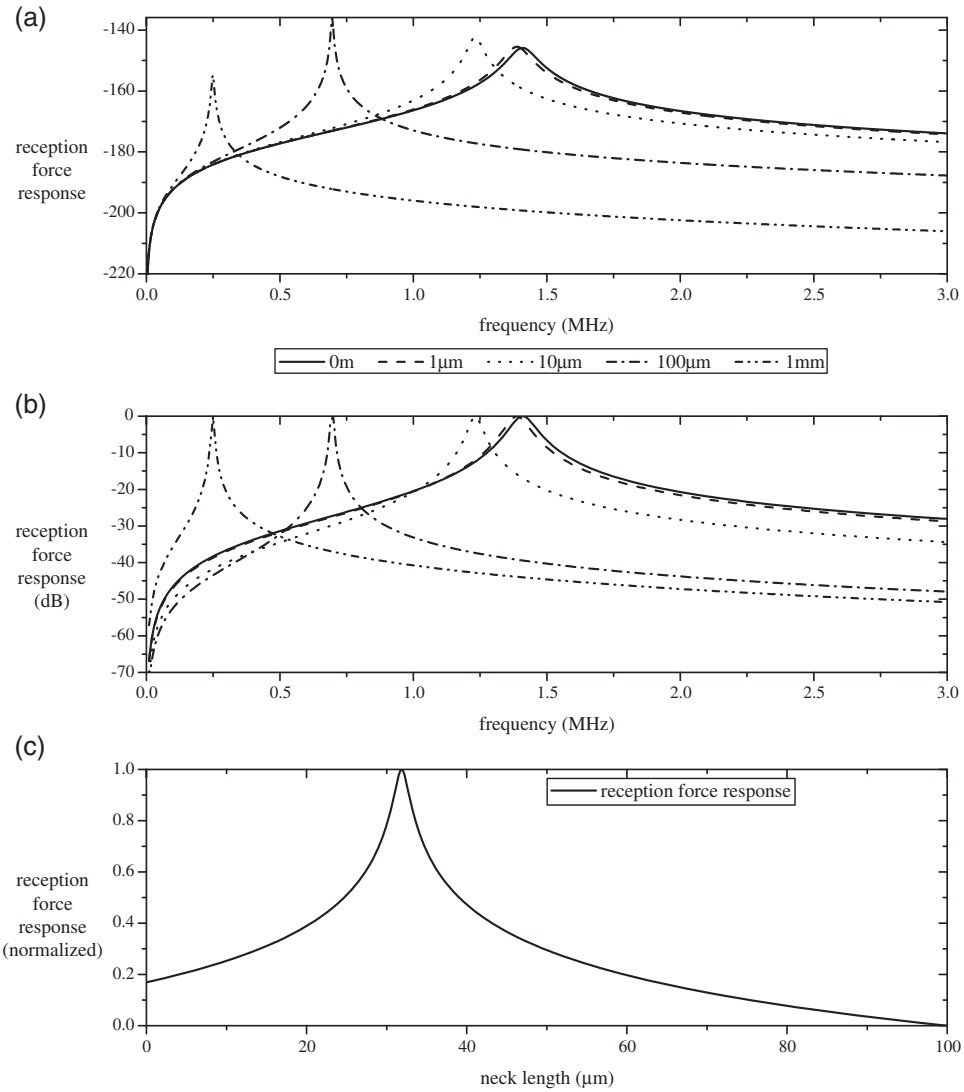

FIG. 10. RFR (a) and normalized RFR in dB (b) of the device, for each of the five values for the neck length. Normalized RFR response as a function of the neck length for fixed frequency $f = 1$ MHz (c).

controlled by selection of the solutes and solvent and the rate of solvent evolution during the deposition process. More specifically, this article focussed on the theoretical modelling of such a device using three different analytical models: a 1D (in space) model, and two 2D (in space) models which consider separate effects on the membrane. The models produced mechanical impedance profiles of the device, in addition to TVRs and RFRs, all of which closely agree.

The 1D pipe-driver model was then used to investigate the effect of changing certain device parameters on the device performance. Specifically, the aperture radius, resonator volume and aperture neck

length were varied. It was observed that the resonant frequency, bandwidth and sensitivity of the device were all highly dependent on these resonator parameters.

Each model showed good agreement and illustrated that the device's performance was highly dependent on the parameters of the backplate. It is therefore important to consider an array of resonators to ascertain if their dimensions could be tailored for specific operating frequencies or bandwidths. As an array of exactly similar resonators has the same impedance as one resonator of the same dimensions, then arrays of resonators of varying dimensions should be studied. There is a possibility of being able to compute array designs which produce outputs with much larger bandwidths than the outputs provided herein. The inverse problem of finding the required parameter values which result in a required operating resonance/bandwidth of the device can also be implemented. The models included could also be used as a guideline for constructing a systems-dynamics model which could prove beneficial for finding optimal parameter values for a specific operating bandwidth and resonant frequency.

Some assumptions were made during the modelling which should be addressed. It was assumed, firstly, that the resonators were equally spaced and identical (although the model itself is constructed in such a manner that this need not be the case). Perhaps more importantly, the model assumed that the membrane, while of the order of size of the backplate, has zero displacement everywhere apart from over each aperture, causing the effective radius of the membrane to be much smaller. Clearly, a free membrane would resonate at a much lower frequencies than the resonant frequency of the backplate, meaning that the device would not operate at its desired frequency. These models must be tested against experimental evidence in order to ascertain if the membrane acts in such a manner.

Furthermore, experimental evidence is required to confirm the model's validity with respect to the operating resonant frequency. In addition, topography scans of the backplate will show to what extent the resonators are of the same shape and dimension. It may be required to introduce a range of sizes of resonators into the model to account for such manufacturing disparities. Furthermore, the actual strength of the pressure output from the models/prototypes must be considered, an aspect which has not been covered in this article. These are experimental issues which are the subject of ongoing investigations.

Finally, there are many facets of these models which could be developed; such as the extent of energy leakage into the silicone substrate and the backplate, the affect of the d.c. bias voltage on device operation and the possibility of filling the resonators with other fluids than air in order to modify the operating frequency. Further methods of comparisons, other than operating frequency, with experimental output will also be considered in future publications.

Acknowledgements

Thanks are given to E. Mackie and R. O'Leary from the Centre For Ultrasonic Engineering, University of Strathclyde, for discussions centred on the experimental work.

Funding

This work was supported by the UK Engineering and Physical Sciences Research Council (EPSRC) (Grant EP/F017421/1). Funding to pay the Open Access publication charges for this article was provided by EPSRC.

References

Álvarez-Arenas, T. E. G. (2004) Acoustic impedance matching of piezoelectric transducers to the air. *IEEE Trans. Ultrason. Ferroelectr. Freq. Control*, **51**, 624–633.

Bayram, B., Hæggström, E., Yaralioglu, G. & Khuri-Yakub, B. T. (2003) A new regime for operating capacitive micromachined ultrasonic transducers. *IEEE Trans. Ultrason. Ferroelectr. Freq. Control*, **50**, 1184–1190.

Campbell, E., Galbraith, W. & Hayward, G. (2006) A new electrostatic transducer incorporating fluidic amplification. *Ultrasonics Symposium*. Vancouver, Canada: IEEE, pp. 1445–1448.

Caronti, A., Caliano, G., Iula, A. & Pappalardo, M. (2002) An accurate model for capacitive micromachined ultrasonic transducers. *IEEE Trans. Ultrason. Ferroelectr. Freq. Control*, **49**, 159–168.

Kinsler, L. E., Frey, A. R., Coppens, A. B. & Sanders, J. V. (2000) *Fundamentals of Acoustics*. Chichester: John Wiley.

Ladabaum, I., Jin, X., Soh, H. T., Atalar, A. & Khuri-Yakub, B. T. (1998) Surface micromachined capacitive ultrasonic transducers. *IEEE Trans. Ultrason. Ferroelectr. Freq. Control*, **45**, 678–690.

Leighton, T. G. (2007) What is ultrasound? *Prog. Biophys. Mol. Biol.,* **93**, 3–83.

Lynnworth, L. C. (1965) Ultrasonic impedance matching from solids to gases. *IEEE Trans. Son. Ultrason.*, **SU-12**, 37–48.

Mackie, E. & O'Leary, R. (2012) Private Communication.

Manthey, W., Kroemer, N. & Mágori, V. (1992) Ultrasonic transducers and transducer arrays for applications in air. *Meas. Sci. Technol.*, **3**, 249–261.

Noble, R. A., Jones, A. D. R., Robertson, T. J., Hitchins, D. A. & Billson, D. R. (2001) Novel, wide bandwidth, micromachined ultrasonic transducers. *IEEE Trans. Ultrason. Ferroelectr. Freq. Control*, **48**, 1495–1507.

Rafiq, M. & Wykes, C. (1991) The performance of capacitive ultrasonic transducers using v-grooved backplates. *Meas. Sci. Technol.*, **2**, 168–174.

Reilly, D. & Hayward, G. (1991) Through air transmission for ultrasonic non-destructive testing. *Ultrasonics Symposium*. Orlando, FL: IEEE, pp. 763–766.

Saffar, S. & Abdullah, A. (2012) Determination of acoustic impedances of multi matching layers for narrowband ultrasonic airborne transducers at frequencies < 2.5 MHz—Application of a genetic algorithm. *Ultrasonics*, **52**, 169–185.

Schindel, D. W., Hutchins, D. A., Zou, L. & Sayer, M. (1995) The design and characterization of micromachined air-coupled capacitance transducers. *IEEE Trans. Ultrason. Ferroelectr. Freq. Control*, **42**, 42–50.

Sneddon, I. N. (1980) *Special Functions of Mathematical Physics and Chemistry*. London and New York: Longman.

Walker, A. J. & Mulholland, A. J. (2010) A theoretical model of an electrostatic ultrasonic transducer incorporating resonating conduits. *IMA J. Appl. Math.*, **75**, 796–810.

Walker, A. J., Mulholland, A. J., Campbell, E. & Hayward, G. (2008) A theoretical model of a new electrostatic transducer incorporating fluidic amplification. *IEEE Ultrasonics Symposium, Beijing, China*, 1409–1412.

Watson, G. N. (1996) *A Treatise on the Theory of Bessel Functions*, 2nd edn. Cambridge: Cambridge University Press.

Weisstein, E. W. (2013) *'Spherical Cap.' From MathWorld–A Wolfram Web Resource.* http://mathworld.wolfram.com/SphericalCap.html. Accessed 26 August 2013.

Wright, M. C. M. (ed.) (2005) *Lecture Notes on the Mathematics of Acoustics*. London: Imperial College Press.

Appendix A. Nomenclature

The tables below provide a full nomenclature of terms used within the article. It is worth noting that, as far as notation concerned, the literature is not consistent and care should be taken when comparing with other work.

Notation	Description
A_m, A_p	Viscous damping
B_m, $\bar{B}_m$, B_p, $\bar{B}_p$, $\hat{B}_p$	Excitation voltage term
C	Capacitance
C_m, $\bar{C}_m$, C_p, $\bar{C}_p$,	Average displacement of membrane term
C_0	Value of capacitance C at $\dot{\Psi} = 0$
c	Speed of sound in resonator
D	flexural rigidity of membrane
d_e	Distance between electrodes
d_m	Thickness of membrane
F	Applied force (in frequency domain)
$f(t)$	Voltage driving force (in time domain)
F_e	Electrostatic force
f_r	Force on membrane
G	Static conductance
h_a	Height of removed cap of spherical resonator
I	Current at electrical inputs
I_n	Modified Bessel function of first kind of nth order
i	Imaginary number
J_n	Bessel function of first kind of nth order
L	Length of neck of resonator
L'	Effective length of neck of resonator
L_m	Distance between lower electrode and membrane
m'	Total effective mass of aperture
N	Number of rows in resonator array
n_j	Number of resonators in row j
P_i	Amplitude of pressure wave on resonator
Pr	Prandtl number
P_o	Pressure produced at membrane load
p_r	Pressure in resonator
RFR, $(\widehat{\text{RFR}})$	Reception force response (RFR in decibels)
R_r	Radiation resistance of resonator
R_v	Damping constant
R_ω	Thermoviscous resistance
r	Radial variable across resonator aperture
r_a	Radius of open aperture in resonator
r_r	Radius of spherical resonator
S_a	Area of aperture of resonator
S_m	Surface area of membrane
s_r	Stiffness of resonator
T	Transduction coefficient
TVR $(\widehat{\text{TVR}})$	Transmission voltage response (TVR in decibels)
t	Time

continued.

Notation	Description
V	Applied voltage (time domain)
V_{ac}	Alternating current voltage
$\bar{V}_{\mathrm{ac}}$	Applied voltage (frequency domain)
V_{dc}	Direct current voltage
V_r	Volume of resonator
x_{dc}	Membrane displacement due to V_{dc}
Y_n	Bessel function of second kind of nth order
Z^b	Acoustic impedance of backplate
Z_{EB}	Blocked electrical impedance
Z_m	Mechanical impedance of transducer
Z_m^l	Mechanical impedance of load
Z_m^b	Mechanical impedance of backplate
Z_m^r	Mechanical impedance of resonator
Z_{mo}	Open-circuit mechanical impedance at $I = 0$.
Z^r	Acoustic impedance of resonator
Z_s ($\hat{Z}_s$)	Combined specific acoustic impedance (Z_s in decibels)
Z_s^l	Specific acoustic impedance of fluid at load
Z_s^r	Specific acoustic impedance of resonator
α_w	Absorption coefficient
β	Ratio of transduction coefficient and electrical impedance
γ_ω	Attenuation coefficient
ϵ_r	Relative permittivity of the membrane
ϵ_0	Permittivity of free space
η	Coefficient of shear viscosity
λ	Wavelength of sound in resonator
ρ_a	Density of fluid in resonator
ρ_s	Density of membrane
τ	Tensile strength of membrane
Ψ	Displacement of membrane (frequency domain)
ψ	Displacement of membrane (time domain)
ω	Angular frequency